


Article

Lab-Scale Investigation of Palm Shell Char as Tar Reforming Catalyst

Yen-Hau Chen ^{1,*} , Max Schmid ¹, Chia-Chi Chang ², Ching-Yuan Chang ² and Günter Scheffknecht ¹

¹ Institute of Combustion and Power Plant Technology, University of Stuttgart, 70569 Stuttgart, Germany; max.schmid@ifk.uni-stuttgart.de (M.S.); guenter.scheffknecht@ifk.uni-stuttgart.de (G.S.)

² Graduate Institute of Environmental Engineering, National Taiwan University, Taipei 106, Taiwan; d92541005@ntu.edu.tw (C.-C.C.); cychang3@ntu.edu.tw (C.-Y.C.)

* Correspondence: yen-hau.chen@ifk.uni-stuttgart.de; Tel.: +49-711-685-69498

Received: 25 March 2020; Accepted: 24 April 2020; Published: 27 April 2020



Abstract: This research investigated the application of palm shell char as a catalyst for the catalytic steam reforming of tar after the sorption enhanced gasification (SEG) process. The catalytic activities of palm shell char and metal-supported palm shell char were tested in a simulated SEG derived syngas with tar model compounds (i.e., toluene and naphthalene) at a concentration of 10 g m⁻³ NTP. The results indicated that palm shell char had an experimentally excellent catalytic activity for tar reforming with toluene and naphthalene conversions of 0.8 in a short residence time of 0.17 s at 900 °C. A theoretical residence time to reach the complete naphthalene conversion was 1.2 s at 900 °C for palm shell char, demonstrating a promising activity similar to wood char and straw char, but better than CaO. It was also found that potassium and iron-loaded palm shell chars exhibited much better catalytic activity than palm shell char, while the parallel reaction of gasification of K-loaded palm shell char influenced the conversion with its drastic mass loss. Moreover, contrary to CaO, palm shell char presented relatively low selectivity to benzene, and its spontaneous gasification generated extra syngas. In summary, the present study demonstrated that the low-cost material, palm shell char, can successfully be used as the tar-reforming catalyst after SEG process.

Keywords: biomass gasification; tar reduction; cost-effective catalytically active biochar; catalytic steam reforming

1. Introduction

Steam gasification is one of the gasification processes for syngas production. An enhanced process, so-called sorption enhanced gasification (SEG), is regarded as an attractive process for hydrogen-rich syngas generation. This process runs in a dual fluidized bed system and is based on a sorption-desorption cycle using calcined limestone (CaO) as the sorbent. In the SEG, the sorbent removes CO₂ from the syngas produced in the gasification reactor at a low-temperature range from 600 °C to 700 °C, resulting in a high hydrogen content in the syngas which hence matches much better for a downstream synthesis (e.g., to produce CH₄ or other products). In a second reactor, the sorbent is regenerated to CaO by heating it via combustion of the remaining char from the gasifier or the additional fuel. The sensible heat of the sorbent that is recycled to the gasifier and the reaction enthalpy of the exothermic CO₂ sorption reaction provide the required reaction heat for the endothermic gasification reactions. The SEG process, covering lab-scale and pilot-scale facilities, has been studied for several years at the Institute of Combustion and Power Plant Technology (IFK), University of Stuttgart [1–3]. In this process, tar production is still a problem because the tar concentration on a dry basis in raw syngas still can reach around 10 g m⁻³_{dry, STP} [4]. However, downstream units, such as gas

engines or turbines require a reduction of the tar content down to $30 \text{ mg m}^{-3}_{\text{dry, STP}}$, or even lower [5]. Tar can be firmly adsorbed on the surface of catalysts for syngas synthesis, inhibiting the production of other chemicals [6–8]. Hence, further tar reduction is necessary, particularly where the syngas is used in synthesis.

Since the raw syngas is produced at a high temperature of 600–700 °C in the SEG process with a high steam concentration, an additional tar reformer loaded with tar cracking catalysts is suitable for coupling with SEG process for tar reduction by steam reforming. This efficient gas cleaning process that can be operated at high temperatures is seen as energetically beneficial. Excessive gas cooling, that is required for condensing and scrubbing of tar in heated syngas, can be avoided. Moreover, tars can be converted into H_2 and CO by steam reforming, promoting the quality of syngas. This study aimed to examine the catalytic steam reforming of tar model compounds, carried in simulated SEG derived syngas, by using low-cost biochars as catalysts that have the potential to be applied in the tar reformer after SEG process.

Although the gas composition from SEG process is dependent on different operation conditions, the ratio of steam volume fraction to hydrogen volume fraction ($V_{\text{H}_2\text{O}}/V_{\text{H}_2}$, -) = 2 in the simulated syngas was chosen in this study, referring to the typical product gas composition in Table 1. Further, gas components, such as CO, CO_2 , methane, and other hydrocarbons were not considered for the tar reforming reaction as the main components in SEG syngas are steam and hydrogen with up to 90 vol %. With a high content of steam in the raw syngas, steam reforming of tar might become the dominant reaction for tar reduction. The composition of tar from the SEG process can be found in Armbrust's research indicating that phenol, toluene, and naphthalene are the major tar components in raw syngas [9]. As phenol is able to be decomposed at high temperatures above 800 °C without any catalysts [10], this study examined the tar reforming with toluene and naphthalene, representing also secondary and tertiary tars [4], of circa $10 \text{ g m}^{-3}_{\text{NTP}}$ based on the typical tar concentration in SEG syngas. Naphthalene concentration around 250 ppmv was considered in this study based on a representative SEG derived tar fraction [8].

Table 1. Typical SEG product gas composition (N_2 free).

Component	Unit	[11,12]	[13]
H_2O	vol %	50–60	60
H_2	vol %	55–71 ^a	26
CO	vol %	5–11 ^a	2.4
CO_2	vol %	7–20 ^a	3
CH_4	vol %	8–13 ^a	5.6
Tar	$\text{g m}^{-3}_{\text{NTP}}$	0.3–3 ^a	1–5

^a On the dry basis.

Ni-based catalysts have been known as commercial catalysts for tar cracking [14,15]. Basically, they are highly efficient in tar conversion. However, Ni-based catalysts are more expensive than active natural materials, and their deactivation occurs easily because of sulfur and heavy tar content in the feed [15,16]. As a result, it is necessary to find other cheap materials that can substitute commercial catalysts, or can be used as a protector to eliminate most of the heavy tar before them. So far, there have been studies indicating that biochars generated by pyrolysis have the ability to decompose organic compounds [17]. These char-based catalysts are comparably low cost and easily available from the biomass fuel and waste by pyrolysis or spent char produced in industrial processes. Moreover, the deactivated char catalyst is easy to handle because of the similar property to the spent char from the gasification process. After the application of tar reduction for SEG process, the replaced char catalysts can be combusted in the regenerator with spent char from the gasifier. On the other hand, char catalysts could be gasified spontaneously during tar reforming, which benefits the syngas production. Based on the above advantages, it is worth studying the application of char-based catalysts for tar reforming after the gasification process.

In this study, palm shell (PS) was considered a potential biomass for producing tar-cracking active biochar by pyrolysis. The production of palm oil has more than doubled in the past two decades, given it is the most widely traded edible oil. In obtaining edible oils from palms, a large amount of PS waste is produced. In recent years, PS waste has been a commercial and cheap biomass to be used as fuel in Asia [18–20]. In addition, activated carbon with high surface area, which is also preferable for tar reforming, can be obtained from palm shell [21]. Consequently, with high production and good properties following carbonization, it is worth investigating the catalytic activity of palm shell char for the special issue of tar reforming and then comparing the catalytic activity with other biochars. According to several references, biochars were manufactured by similar methods for the purpose of tar reforming. For example, (1) biochar was prepared by pyrolyzing pine bark at 950 °C for 2 h with nitrogen [22]; (2) pyrolysis of sawdust was carried out in 2.0 L min^{−1} Ar atmosphere at a slow heating rate of 10 °C min^{−1} and a final pyrolysis temperature of 800 °C with the residence time 30 min [23]; (3) rice husk was then pyrolyzed with a slow heating rate of 10 °C min^{−1} to a final pyrolysis temperature of 800 °C. The hold time was 10 min [24]. This study then established a pyrolysis procedure for the manufacturing of palm shell char according to the above methods.

The mechanism of tar cracking on biochars has also been studied recently. Feng et al. pointed out that the main factors of tar reforming are highly related to alkali and alkaline earth metal (AAEMs) contents, and the surface area of biochar [24–26]. The reaction mechanism of tar reforming with AAEMs species on biochar is comprehensively explained in their research. The presence of K and Ca elements, which lead to repeated bond-forming and bond-breaking of tar fragments, contributes to tar decomposition and the formation of light hydrocarbons and small-molecule gases. Apart from AAEM groups, Klinghoffer et al. also found that Fe sites on the char surface react obviously as active sites for the catalytic reaction. The high carbon deposition was found on the Fe site on char after applying char as a decomposing catalyst for organic compounds [27]. Kastner et al. [28] also pointed out that iron might be reduced to metallic iron (Fe) or other forms of more reduced iron (e.g., FeO) via hydrogen during steam reforming of toluene over Fe supported biochar, which is beneficial to toluene reforming as it has been already confirmed that iron in reduced forms can catalytically decompose tar [29]. This study investigated the reforming ability of potassium in tar and iron-loaded palm shell chars. Another low-cost material, CaO, which is used as the sorbent in the SEG process, was also tested here as the reference catalyst, as compared with biochar catalysts. Since Chen et al. found that CaO performed well on toluene cracking through steam reforming [30], CaO might be applicable as the tar-reforming catalyst in a downstream reformer after SEG process. For better understanding the role of individual catalysts, sole catalyst-sorbents were examined. This information provides the basic knowledge for further testing the possibility of using mixed catalyst-sorbents, which would complicate the preparation of catalysts.

2. Results

2.1. Characteristics of Palm Shell Char (PSC), 5%K-Loaded Palm Shell Char (5%K-PSC), 5%Fe-Loaded Palm Shell Char (5%Fe-PSC), Wood Char (WC), and Straw Char (SC)

All bio-chars were manufactured by the pyrolysis process described in Section 3.1. According to Table 2, after the pyrolysis of PS, its contents of equilibrium moisture and volatile matters decreased significantly, while that of fixed carbon content increased, as expected. Since the higher volatile matter makes biomass more susceptible to tar formation during steam reforming, the low content of only 3.4 wt.% in PSC is suitable for the following tar-reforming catalyst usage. Fixed carbon and carbon content increased from 4.7 to 89.7 wt.%, and from 38.8 to 89.8 wt.%, respectively, proving that the carbonization during pyrolysis increased carbon content. According to Klinghoffer et al. [31], the presence of carbon in biochar promoted the catalytic activity. After intense carbonization by pyrolysis, the performance of tar reforming over PSC and WC might be enhanced. It was also found that PSC had much lower oxygen content of 1.82 wt.% compared to that of PS of 35.3 wt.%, suggesting that more hydrophobic solid was formed after pyrolysis [32].

Both K and Fe-supported PSC had higher ash contents of 16.9 wt.%, and 17.8 wt.%, respectively, than PSC with 4.61 wt.%. After PSC was impregnated with potassium and iron-containing solutions, 11.0 wt.% of K₂O and 12.1 wt.% of Fe₂O₃ were observed by metal analysis in 5%K-PSC and 5%Fe-PSC, respectively, while PSC had only 0.532 wt.% of K₂O and 0.939 wt.% of Fe₂O₃ in ash. These results verify that the metal loading method used in this study can successfully load potassium or iron on the PSC. Although ash content had a significant rise after PS was soaked with K and Fe, the major component in both, metal-loaded PSC is still carbon, as can be seen in Table 2.

Among three biochars produced from palm shell, wood, and straw, SC had the highest ash content of 31.1 wt.% resulting in the lowest carbon content among three biochars. In comparison to PSC and WC, SC possessed more AAEM contents, which can promote the activity of biochars for gasification and tar reforming [24,33]. Moreover, the equilibrium moisture content of PSC was only 2.0 wt.% much lower than those of WC and SC with a value of around 7 wt.%, which was better for storage and transportation when applying it as catalysts.

PSC possessed a much higher BET surface area (469.6 m² g⁻¹) compared to that of CaO with only 8.8 m² g⁻¹. However, a negative effect of potassium was found in the pyrolysis process for producing char catalysts. Char lumps were formed from the individual pellet, which might be caused by the agglomeration of potassium. At such a high temperature as in this case, excessive impregnation of potassium on biochar can lead to agglomeration during pyrolysis [34]. A blockage in the pyrolyzer was observed, causing the difficulty of manufacturing K-loaded PSC. According to the surface area analysis of three PSCs, 5%K-PSC has a tiny surface area of 6.9 m² g⁻¹, which might be due to agglomeration, resulting in the disappearance of the porous structure, while the surface areas of 5%Fe-PSC and PSC are both above 200 m² g⁻¹ shown in Table 2.

Table 2. Characteristics of PS, PSC, 5%K-PSC, 5%Fe-PSC, WC, and SC.

Analyses	Compositions	PS ^c	PSC	5%K-PSC	5%Fe-PSC	WC	SC
Proximate Analysis ^a (wt.%)	Fixed carbon	4.73	89.7	59.8	69.3	77.54	53.5
	Volatile matters	80.21	3.38	13.4	7.32	10.50	8.09
	Ash	2.64	4.61	16.9	17.8	5.36	31.1
	Equilibrium moisture ^b	12.42	2.00	9.94	5.58	6.58	7.30
Ultimate Analysis ^a (wt.%)	C	38.8	89.8	67.5	75.3	83.8	56.7
	H	6.00	0.708	1.70	0.974	1.23	1.15
	O	35.3	1.82 ^d	3.02 ^d	-	2.57 ^d	1.81 ^d
	N	0.298	0.905	0.873	0.745	0.428	1.02
	S	0.038	0.075	0.017	0.047	0.009	0.345
	Cl	0.044	0.079	0.047	0.028	0.020	0.579
Ash components ^a (wt.%)	Al ₂ O ₃	-	1.72	0.014	0.058	0.095	0.407
	BaO	-	0.004	0.0001	0.0001	0.019	0.008
	CaO	-	0.215	0.430	2.08	2.03	1.62
	Fe ₂ O ₃	-	0.939	0.021	12.1	0.059	0.656
	K ₂ O	-	0.532	11.0	0.340	1.24	4.24
	MgO	-	0.054	0.057	0.087	0.342	1.10
	MnO ₂	-	0.002	0.004	0.020	0.255	0.525
	Na ₂ O	-	0.060	0.033	0.016	0.014	0.685
	P ₂ O ₅	-	0.028	0.029	0.045	0.215	0.731
	SO ₃	-	0.17	0.031	0.071	0.008	0.803
	SiO ₂	-	3.22	1.74	2.68	0.656	18.1
	SrO	-	0.008	0.001	0.002	0.006	0.005
	TiO ₂	-	0.077	0.001	0.00	0.004	0.028
BET total surface area (m ² /g)		-	469.6	6.93	220.7	-	-

^a In wet basis. ^b Equilibrium moisture content of sample in air. ^c Data of the report [35]. ^d Balance of C, H, N, S, Cl, equilibrium moisture, and ash.

It is essential to predict the remaining mass from the pyrolysis of PS for catalyst production. Therefore, thermal gravimetric analysis (TGA) and derivative thermal gravimetric analysis (DTG) of PS, in an N₂ environment, were carried out to analyze weight loss with increasing temperature.

Since metal impregnation might influence the pyrolysis rate of biomass, it is also worth understanding the effect of K and Fe on the pyrolysis of PS. Generally, hemicellulose has a sharp pyrolysis rate of around 277–312 °C [32]. As soon as arriving at 355 °C, the intense decomposition of cellulose can be observed. However, decomposition of lignin would be difficult to be identified because of overlapping temperatures with cellulose. Figure 1 presents the temperature variation of the residual mass fraction (M_R) of PS, 5%K-PS, and 5%Fe-PS in TGA curves. It shows K and Fe reduce the required temperature for the decomposition of PS while Fe-impregnated PS starts to have apparent weight loss at a much lower temperature of around 206 °C than K-impregnated PS at 254 °C. The first and second peaks (P1 and P2) of DTG curves of 5%K-PS and 5%Fe-PS are all at lower temperatures (temperatures of P1 and P2 of 5%K-PS = 266 °C and 332 °C; temperatures of P1 and P2 of 5%Fe-PS = 277 °C and 341 °C) compared to those of PS (temperatures of P1 and P2 of PS = 284 °C and 361 °C), indicating that the pyrolysis temperature of iron- and potassium-loaded PS can be conducted at lower temperatures for converting the hemicellulose and cellulose of PS into liquids and gases. The TGA results indicate that PS, through the first step pyrolysis at 450 °C in the manufacturing process of this study, had a significant mass loss, and most volatiles was removed at this stage. Then, the increase in temperature to 850 °C caused only a little drop in the mass. Eventually, TGA curves tend to $M_R = 0.3$ – 0.4 at 850 °C for three types of PSs, which gives a rough concept for PSC production by pyrolysis of PS.

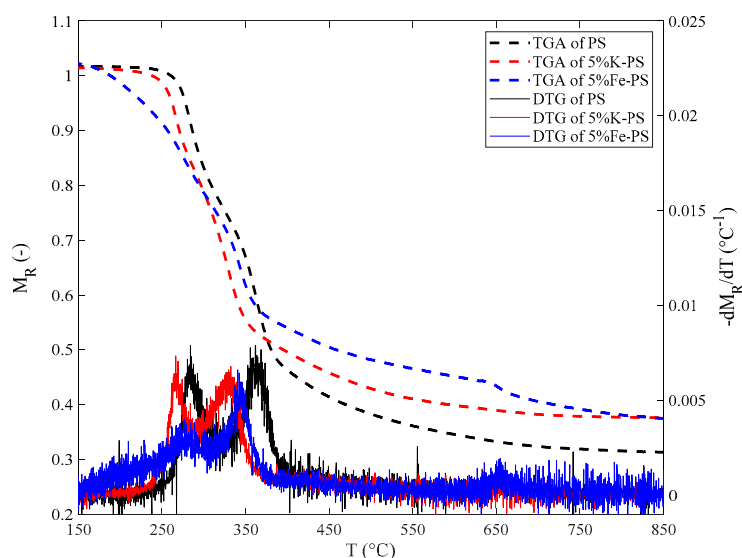


Figure 1. TGA and DTG diagrams from pyrolysis of PS, 5%K-PS, and 5%Fe-PS of residual mass fraction (M_R) and $-dM_R/dT$ vs. temperature at heating rate = 30 °C min^{−1} in N₂.

2.2. Tar Reforming over PSC, WC, and SC

2.2.1. Conversions of Tar and Gasification Rates of PSC at Different Temperatures

In 90 min reforming of tar model compounds over PSC, the trends of toluene (X_T , -) and naphthalene conversion (X_N , -) at 850 °C and 900 °C are depicted in Figure 2. It is apparent that higher X_T and X_N of roughly 0.8 can be reached at 900 °C at the end of testing. However, conversions needed some time to approach the stable state from low conversions. This phenomenon was also observed when using WC and SC as catalysts (shown in Section 2.2.2). For example, X_N at 900 °C in Figure 2, increases from 0.24 to 0.80 during the initial 15 min, which suggests that the catalytic activity can be enhanced in this time range. After pyrolysis, high porosity is not accessible as the pores fill from disorganized carbon from the deposited tar, which reduces the surface area and pore distribution on the char surface [36]. However, with a high content of steam and high temperature during tar reforming, the gasification of char can take place and change the surface property of chars. According

to Fuentes-Cano et al. [37], when the rate of carbon (char and soot) gasification is higher than that of coking during tar reforming, the surface area and porosity of the char are increased, resulting in a better activity of the char. Consequently, with high steam content in SEG derived syngas, the steam activation process (gasification) for more surface area of chars might be directly carried out at elevated temperatures during tar reforming. In order to verify this phenomenon, a method was established here, for presenting the gasification of palm shell char during the reforming of tar model, compounds. The gasification rate (r_G , g min^{-1}) of the char was then calculated here during 90 min reforming.

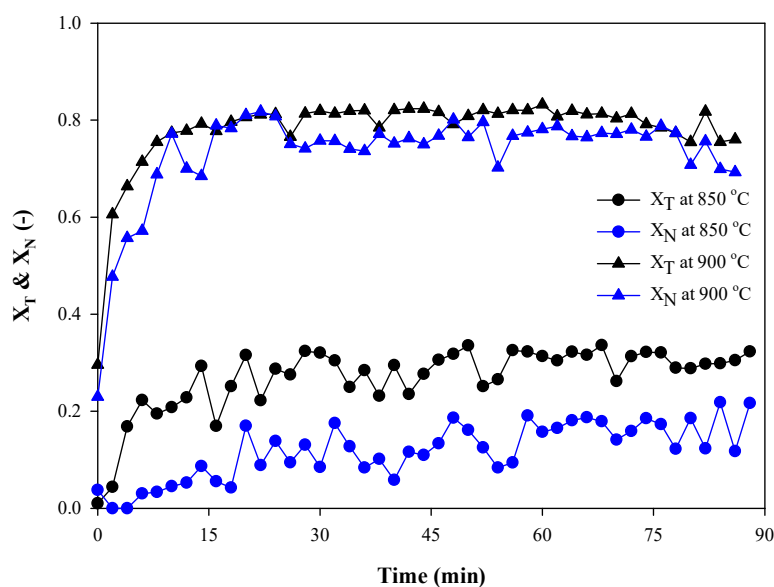


Figure 2. Conversions during 90 min tar reforming over PSC.

r_G of PSC is defined as the rate of reacted carbon from PSC, while r_G can also be assumed equal to the rate of production of CO and CO₂ stemming from PSC presented in Equation (1) on the basis of gasification reactions as shown in Equations (13) and (18) (Reactions are described in Section 3.5) [38], where m_{C^*} , m_{C_CO} , and $m_{C_CO_2}$ (g) are the mass of carbon in the char, in the produced CO, and in the produced CO₂ at time t , respectively:

$$r_G = \frac{-dm_{C^*}}{dt} = \frac{d(m_{C_CO} + m_{C_CO_2})}{dt}. \quad (1)$$

m_{C_CO} and $m_{C_CO_2}$ at time t are computed by the integration of volume fractions of CO and CO₂ arising from PSC gasification (y_{G_CO} and $y_{G_CO_2}$, ppmv) with t , which is substituted into the ideal gas Equation at NTP (assuming CO and CO₂ are ideal gases), according to Equations (2) and (3):

$$m_{C_CO} = \frac{P\bar{M}V}{RT} = \frac{P\bar{M}}{RT} \times (\dot{Q}_{NTP} \times \int_0^t y_{G_CO} dt) \quad (2)$$

$$m_{C_CO_2} = \frac{P\bar{M}V}{RT} = \frac{P\bar{M}}{RT} \times (\dot{Q}_{NTP} \times \int_0^t y_{G_CO_2} dt), \quad (3)$$

where P is pressure (assumed at 101.3 kPa), \bar{M} is the molar mass of carbon (12 g mol^{-1}), R is the ideal gas constant ($8.314 \text{ Pa}\cdot\text{m}^3\cdot\text{K}^{-1}\cdot\text{mol}^{-1}$), temperature (T) is 298 K here, and $\dot{Q}_{NTP} = 0.3 \text{ m}^3 \text{ h}^{-1} = 5 \text{ L min}^{-1}$ at NTP.

y_{G_CO} and $y_{G_CO_2}$ can not be directly obtained from the outlet volume concentration of CO and CO₂ (y_{CO} and y_{CO_2} , ppmv) detected by FTIR because toluene and naphthalene also contributed to CO and CO₂ production due to Equations (11), (12), and (13). As a result, they are enumerated by

y_{CO} and y_{CO_2} subtracting concentrations of CO and CO₂ from tar model components (y_{T_CO} and $y_{T_CO_2}$, ppmv) at time t , presented as Equation (4). This method assumes that PSC only converted into CO and CO₂ (the main product of gasification of PSC from Equations (13) and (18)) during 90 min reforming, and carbon-containing species of products from the conversion of tar model components existed only as CO, CO₂, C₆H₆, and CH₄. Hence, C₇H₈, C₁₀H₈, CH₄, and C₆H₆ analyzed by FTIR were all assumed originating from the infused tar model compounds. y_{T_CO} and $y_{T_CO_2}$ can be then calculated by fractions of C from reacted toluene and naphthalene deducting those from CH₄ and C₆H₆ (Equation (5)). The gasification rate of PSC during reforming of tar model compounds at time t is subsequently calculated by Equations (1), (2), and (3). Finally, r_G of PSC at 850 and 900 °C against time is then illustrated in Figure 3:

$$y_{G_CO} + y_{G_CO_2} = y_{CO} + y_{CO_2} - (y_{T_CO} + y_{T_CO_2}) \quad (4)$$

$$y_{T_CO} + y_{T_CO_2} = 7 \times (y_{C_7H_8, in} - y_{C_7H_8}) + 10 \times (y_{C_{10}H_8, in} - y_{C_{10}H_8}) - 6 \times y_{C_6H_6} - y_{CH_4}. \quad (5)$$

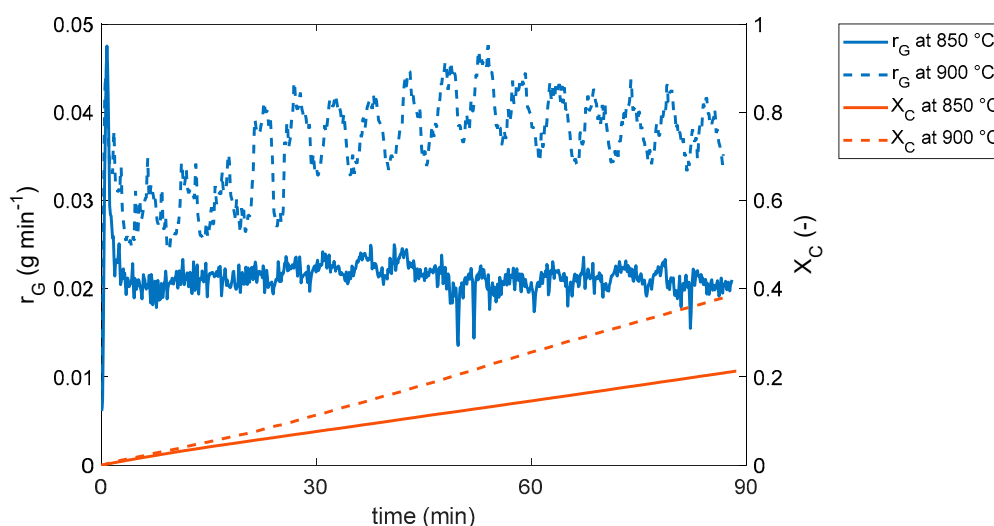


Figure 3. Comparison of calculated r_G and X_C during 90 min tar reforming over PSC.

The conversions of carbon mass (X_C , -) of PSC is also calculated also by this method. By Equations (2) and (3), the mass of carbon in PSC transforming to CO and CO₂ ($m_{C_CO} + m_{C_CO_2}$) is obtained, so X_C at time t can be calculated by Equation (6) and illustrated in also Figure 3, where M_C is the initial carbon mass in the biochar (g). The diagram shows that carbon in PSC is gasified apparently in 90 min test with $X_C = 0.20$ and 0.40 at 850 and 900 °C, respectively. The error of this method is estimated by the difference between X_C calculated from this method and real X_C . The real X_C after 90 min reforming ($X_{C,real}$, -) is calculated by the mass loss (Δm , g) of PSC measured after the experiment divided by M_C (Equation (7)). X_C at 90 min (= 0.20 and 0.40) has an excellent compromise to $X_{C,real}$ (= 0.20 and 0.45) at 850 and 900 °C suggesting this method can be used for constructing the first concept of mass loss of carbon catalysts during steam reforming of tar. This method is also helpful for the establishment of the change of the residence time in the course of tar reforming:

$$X_C = \frac{m_{C_CO} + m_{C_CO_2}}{M_C} \quad (6)$$

$$X_{C_real} = \frac{\Delta m}{M_C}. \quad (7)$$

According to Figure 3, a higher gasification rate can be observed at 900 °C in 90 min reforming with a constant $r_G = 0.039$ higher than $r_G = 0.022$ g min⁻¹ at 850 °C. Hence, more surface area and pore volume might be formed at 900 °C, while twice the loss of carbon mass occurs compared to 850 °C in 90 min. In order to figure out the relationship between gasification and surface area, the result of internal structure analyses is shown in Table 3. After 850 °C reforming, the surface area and micropore area all increase. With strong gasification at 900 °C reforming, the surface area and the micropore surface area become more than 850 °C reforming, which is consistent with the previous hypothesis that gasification activates the char surface and high gasification rate leads to more surface area and micropores. However, the ratio of micropore to mesopore area has a decrease from 5 to 2 after 900 °C tar reforming, indicating a possible micropore collapsing through long-time strong gasification. This phenomenon, which is related to the deactivation of char catalyst, was also found by Zeng et al. [39].

Table 3. The internal structure of PSC and PSCs after 90 min test.

Sample	BET Total Surface Area (m ² g ⁻¹)	Micropore Area (m ² g ⁻¹)	Mesopore Area (m ² g ⁻¹)	The Ratio of Micropore to Mesopore Area	Micropore Volume (cm ³ g ⁻¹)	Pore Average Diameter (nm)
PSC	469.6	331.8	66.1	5.0	0.199	2.5
PSC-850	532.6	430.1	82.0	5.2	0.2	2.13
PSC-900	813.7	511.3	253.1	2.0	0.26	2.68

2.2.2. Comparison of Conversions of Tar and Gasification Rates between PSC, WC, and SC

X_N of naphthalene reforming over PSC, WC, and SC is depicted in Figure 4, which illustrates that naphthalene reforming over wood char presenting the best activity of naphthalene reforming at 850 °C in the whole 90 min. Here only X_N is depicted in Figure 4 to avoid the interference of showing toluene conversions. The toluene conversion trends, from each biochar, also indicated that WC had the best catalytic activity at 850 °C. The method described in Section 2.2.1 was also adopted to 90 min reforming of tar model compounds over WC and SC to compare the gasification rate and carbon conversion of different biochars. Due to the difference in bulk density of different biochars, r_G is then divided by individual M_C (r_G/M_C , min⁻¹) of them for the comparable rate of gasification. Figure 5 shows that SC has the most drastic gasification with $X_C = 0.60$ in 90 min reforming, which may be due to the highest ash content among these three biochars with abundant AAEM groups. Some research has confirmed that AAEM groups enhance the gasification rate of biochars [40,41]. This surmise also agrees with WC, which is more susceptible to steam for gasification with $X_C = 0.35$ in 90 min reforming than PSC because of a higher content of AAEM groups. With the least content of AAEM groups, r_G/M_C of PSC remains almost constant during the whole time reforming range. At 850 °C, X_C at 90 min of PSC (=0.21) is much lower than those of WC and SC, demonstrating a stabilized characteristic at high temperature and rich steam concentration environments.

In light of Figure 5, the primary gasification of WC and SC takes place in the beginning, and r_G/M_C becomes constant afterward. The surface area might soar tensely in this gasification time range, explaining the increase of activity of biochars at the starting time range, as can be seen in Figure 4. This study also proves that biochar catalysts can be parallelly gasified to raise the amount of H₂ and CO to increase their contents in the bio-syngas during the reforming of tar model compounds.

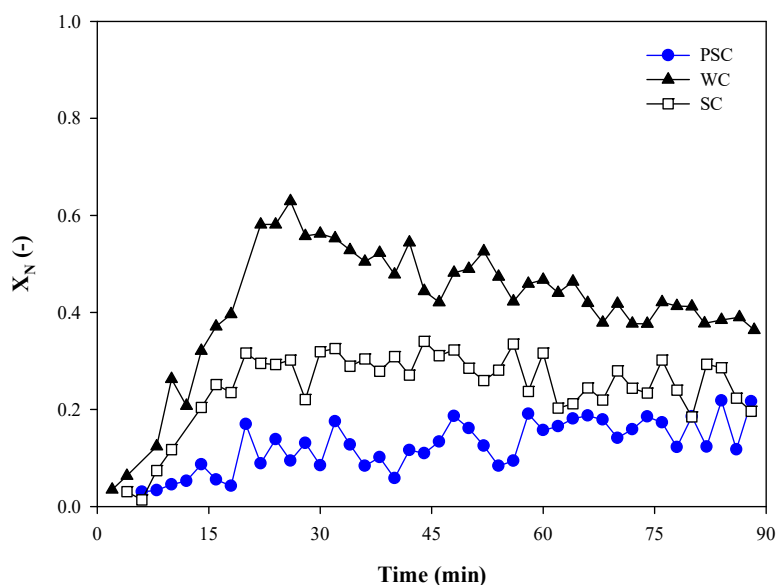


Figure 4. Naphthalene conversions during 90 min tar reforming over PSC, WC, and SC at 850 °C.

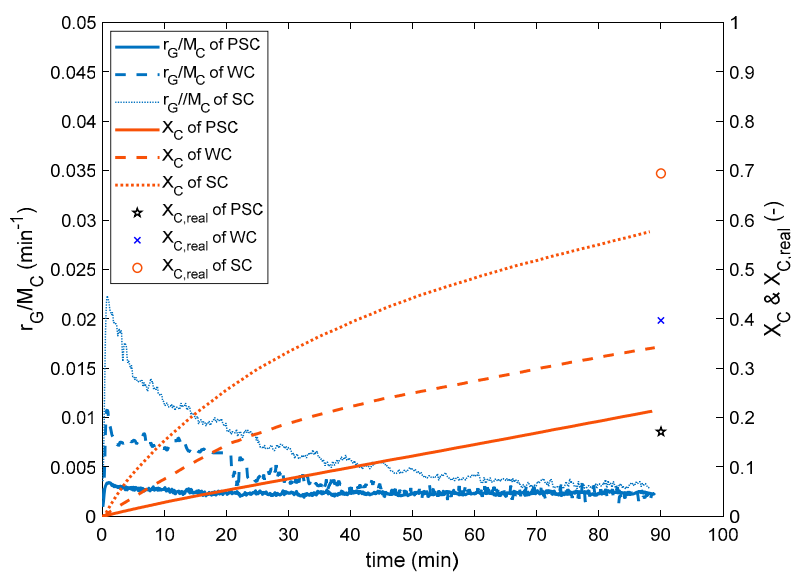


Figure 5. Comparison of calculated r_G/M_C and X_C during 90 min tar reforming over PSC, WC, and SC at 850 °C.

2.3. Tar Reforming over 5%K-PSC and 5%Fe-PSC

Loading metal on biochars is a time-consuming process with extra cost, so quick mass loss of biochar catalysts due to gasification should be avoided in a long-duration reaction. A drastic mass loss also means a decrease in residence time. Therefore, tar conversion can drop. According to reference [40], impregnated potassium and iron can significantly increase the gasification rate of the biochar. A continuous three-stage tar reforming at three temperatures was thus conducted to investigate the effect of T and r_G/M_C on tar conversion. At different stages, only nitrogen went through the reformer. As soon as the stage temperature was reached and maintained constant, simulated syngas with tar model compounds then flowed into the reformer for roughly 8 min reforming. r_G/M_C , X_C , and X_N in three stages for 5%K-PSC and 5%Fe-PSC are depicted in Figure 6a,b. A significant difference in the gasification rate between iron- and potassium-loaded chars was thus observed in this research.

At each stage, steam activation of Fe-loaded PSC quickly occurs with an extremely high gasification rate in the beginning, while the mass loss is much less than 5%K-PSC during long-term reforming on account of a rapid drop of r_G/M_C . Regarding the reforming of tar model compounds at 840 °C as an example, 5%Fe-PSC has a considerable decrease of r_G/M_C from 0.035 to 0.003 min^{-1} , and the value then maintains constant close to r_G/M_C of PSC depicted in Figure 5. According to Yu et al. [42], iron in its reduced forms on the char surface can be oxidized into magnetite during short reforming time with steam, which reduces the activity of char for reacting with steam and hence leads to a sink of r_G/M_C . In contrast, with potassium on the surface of PSC, a high gasification rate, which is twelve times greater than that of PSC at 850 °C, appears with nearly a constant value through the reforming.

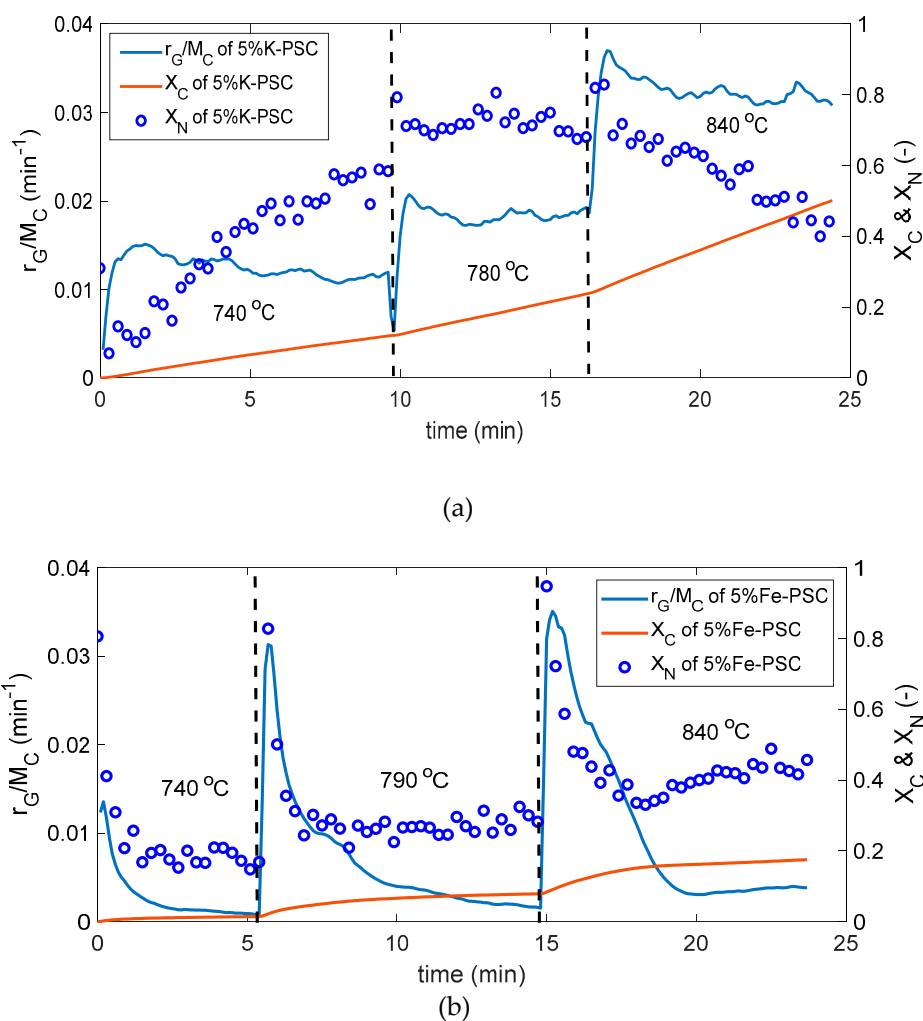


Figure 6. The tendency of calculated r_G/M_C and X_N during tar reforming over; (a) 5%K-PSC; and (b) 5%Fe-PSC at a continuous three-stage tar reforming.

X_N has a rapid increase to 0.54 at the first stage due to the strong steam activation of 5%K-PSC. At the second stage, conversion approaches a much higher value of 0.70. However, a considerable drop of X_N at 850 °C is found. This is not consistent with the general trend of K-loaded char in other research [43], which suggests that conversion increases along with rising temperatures. Through three stages, the carbon conversion of 5%K-PSC quickly reaches 0.5 in only 24 min. Therefore, the enormous mass loss of 5%K-PSC through three-stage reforming might be the main reason for the conversion drop with the need for fast replacement of the catalyst. According to the references [39,44], although new micropores can be formed on biochars during gasification, it is found that micropores can further

collapse to mesopore because of continuously intense gasification. Since the activity of tar reforming is highly related to the micropore of biochar [39], in the long term or drastic gasification situation, pore collapsing might also lead to deactivation. With the highest gasification rate at the final stage where naphthalene conversion starts to decrease, an intense gasification rate might also result in the collapse of micropores. In comparison to 5%K-PSC, the X_C value of 5%Fe-PSC is only 0.19 at the end of three-stage reforming without the decline of naphthalene conversion.

As a result, rapid mass loss of char catalysts because of gasification during tar reforming must be avoided to maintain the activity of char catalysts. In the site of reforming at a low temperature of 750 °C, the gasification rate of K-loaded PSC is still much faster than that of PSC at 850 °C. Consequently, the proper temperature (below 750 °C) should be considered to reduce the severe mass loss of 5%K-loaded PSC while applying them as a catalyst in tar reforming.

Although potassium has been commonly tested as a promoter for char catalyst, agglomeration in pyrolysis for the catalyst production and strong gasification during tar reforming have to be considered as problems. Iron is a relatively tender promoter on the biochar suitable for long-term operation with a quick activation only at the very beginning during the reforming of tar model compounds. However, this research only gives a general concept for applying metal-supported biochars in tar reforming. Further investigation of these metal-loaded PSCs should still be carried out.

2.4. Catalytic Activities of Different Biochar at Different Temperatures

By sorting average conversions at different temperatures, the catalytic activities of the reforming of tar model compounds over all biochars are compared here. As can be seen in Figure 7, conversions of both, toluene and naphthalene over WC, SC, and PSC are observed at temperatures above 800 °C, where WC has the best catalytic activity for tar reforming with the highest X_T and X_N of roughly 0.7 at 880 °C in $\tau_{NTP} = 0.17$ s. On the other hand, X_T and X_N increase along with the temperature, suggesting that naphthalene and toluene can be better reformed at high temperatures.

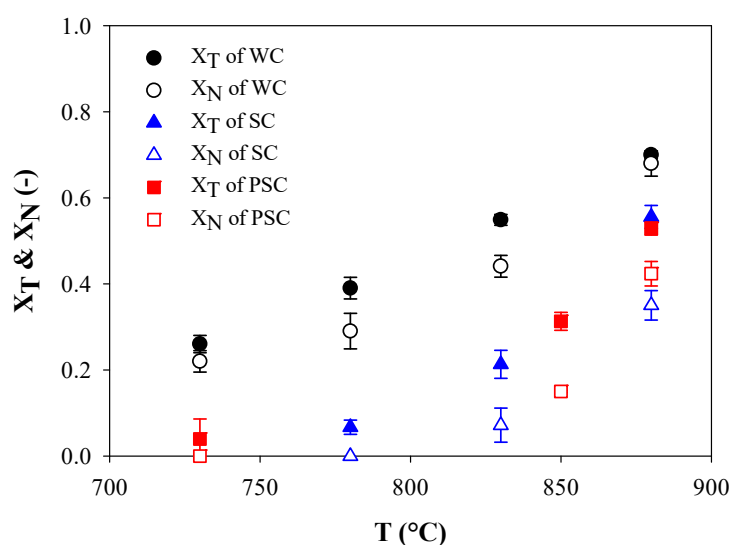


Figure 7. X_T and X_N from tar reforming over PSC, WC, and SC at different temperatures.

The average conversions of 5%K- and 5%Fe-PSC from the tests in Figure 6 are depicted in order to understand whether conversion can be enhanced in the presence of additional K and Fe. Figure 8 shows that 5%K-PSC has an excellent catalytic activity with high X_T and $X_N = 0.7$ at moderate temperature = 780 °C. However, both conversions decrease to 0.54, and 0.47, respectively, at 840 °C, caused by rapidly decreasing char amount owing to drastic char gasification, which has been explained in Section 2.3. With the iron on the surface, the catalytic activity was also promoted,

giving higher conversions of toluene and naphthalene than PSC. These findings correspond to the references [24–26,28] that potassium and iron enhance the ability of tar decomposition over biochars in a steam-hydrogen rich environment.

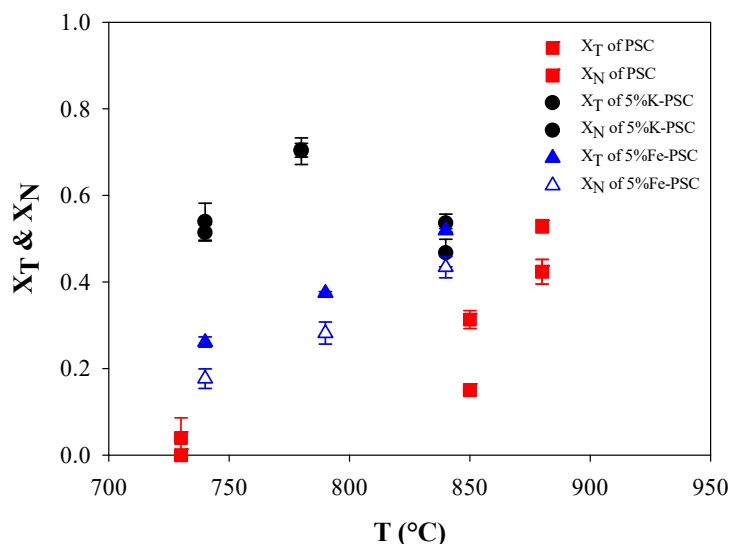


Figure 8. X_T and X_N from tar reforming over PSC, 5%K-PSC, and 5%Fe-PSC at different temperatures.

According to references [45,46], char-based catalysts have been reported that the content of oxygen-containing functional groups on the surface enhanced its activity for tar reforming. These groups were mainly in the acidic form and increased the acidity of the char-based catalyst [47]. Therefore, the acidity of the char-based catalyst is then regarded as an essential characteristic for improving the removal efficiency of tar. Since the tar-reforming activity of PSC was enhanced after dopped with K and Fe, the acidity on the surface of 5%K-PSC and 5%Fe-PSC might be higher compared to PSC. Hazmi et al. also indicated that after moderate impregnation of K and Fe on the rice husk char, a significant increase of the acidity was observed on its surface [48].

2.5. Benzene Selectivities of Different Biochars

Benzene has been known as an intermediate which is cracked mainly from aromatic tars through dealkylation. With better catalysts, benzene can be further decomposed to light gas components indicating that benzene selectivity ($S_{C_6H_6}$, -) can also be regarded as a proper index to evaluate whether tar tends to decompose to light gas components with certain catalysts or not. Figure 9 shows that $S_{C_6H_6}$ of three different PSCs are smaller than 0.2 compared to relatively high values between 0.20 and 0.54 obtained from CaO in the temperature range from 700 to 900 °C. Moreover, the reforming of tar model compounds over WC and SC also exhibited similar selectivity of benzene with values below 0.2, suggesting that biochars are inclined to break down benzene further and present high selectivity to light components due to unique surface possessing AAEM groups. In addition, apparent drops of $S_{C_6H_6}$ of PSC and CaO occur at 850 °C to 900 °C, meaning that, at a high-temperature range above 850 °C, not only high conversion rate can be approached over PSC and CaO, but benzene is also much easier to decompose.

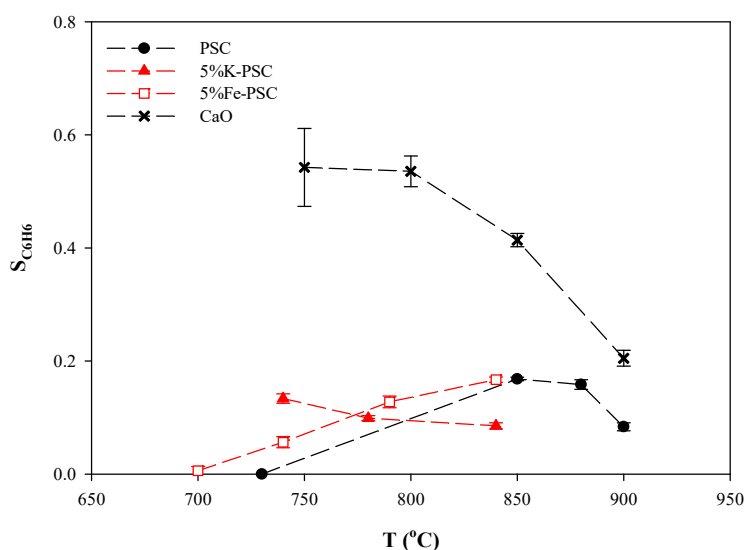


Figure 9. $S_{C_6H_6}$ of PSC, 5%K-PSC, 5%Fe-PSC, and CaO at different temperatures.

2.6. Kinetics

Kinetic constants can be calculated using kinetic models, along with the relationship between tar concentration and reaction temperature. In a recent review paper [17], the kinetics of tar model compounds reforming over char catalysts were assessed from the previous publication. It indicated that the research on reaction kinetics of tar removal is very scarce at present. Generally, for the typical tar model compounds, such as phenol, toluene, and naphthalene, the first-order reaction model is appropriate in describing the reaction process. By using the same model, it is also beneficial for comparing the results with the literature [22,49]. As a result, the first-order kinetic model presented in Equation (8) was then applied in this study,

$$-r = k \cdot C_{tar} \quad (8)$$

where r is the rate of model tar conversion ($\text{kmol m}^{-3} \text{s}^{-1}$), k is the apparent kinetic constant (s^{-1}) and C_{tar} is the model tar concentration (kmol m^{-3}). The validity of the model can be justified by the R-square value (R^2 , -) of the model fitting with data.

Plug-flow behavior and negligible diffusion in the catalyst pellets are assumed for determining the kinetic parameters. k is then integrated as below,

$$k = \frac{\ln(1 - X)}{\tau_{NTP}} \quad (9)$$

where X is the conversion of tar model compounds (-), and τ_{NTP} is the gas residence time (s) in the catalytic bed based on gas flow rate. X of materials at different temperatures is based on Figures 7 and 8. For 5%K-PSC, the conversions at 840 °C were excluded due to the intense gasification of char.

By substituting respective k and reforming temperature (T_r , k) into Arrhenius' law (Equation (9)), the activation energy (E_a , kJ/mol) (assumed to be constant in the studied temperature range) and the apparent pre-exponential factor (k_0) can be computed. Then both kinetic parameters can be compared with the results of other researchers to evaluate the activity of the applied catalysts for tar reforming,

$$k = k_0 \cdot e^{\frac{-E_a}{R \cdot T_r}} \quad (10)$$

where R is the ideal gas constant ($8.314 \text{ J K}^{-1} \text{ mol}^{-1}$).

The apparent rate constant was varied with temperature by an Arrhenius-type relationship, as shown in Figure 10. Linear regressions were then established for toluene and naphthalene reforming over different materials based on the Arrhenius-type relationship. According to Table 4, high R^2 , which are derived from these linear regressions, confirmed a good fit for the first-order kinetic model. With two parameters E_a and k_0 , as listed in Table 4, the performance of different active materials, tested in this study, can be easily compared by establishing the relationship between residence time and conversion (Figures 11–13). 850 °C and 900 °C were selected as the standard temperatures for the comparison of catalytic activity of natural materials because they have been regarded as effective temperatures for tar reforming.

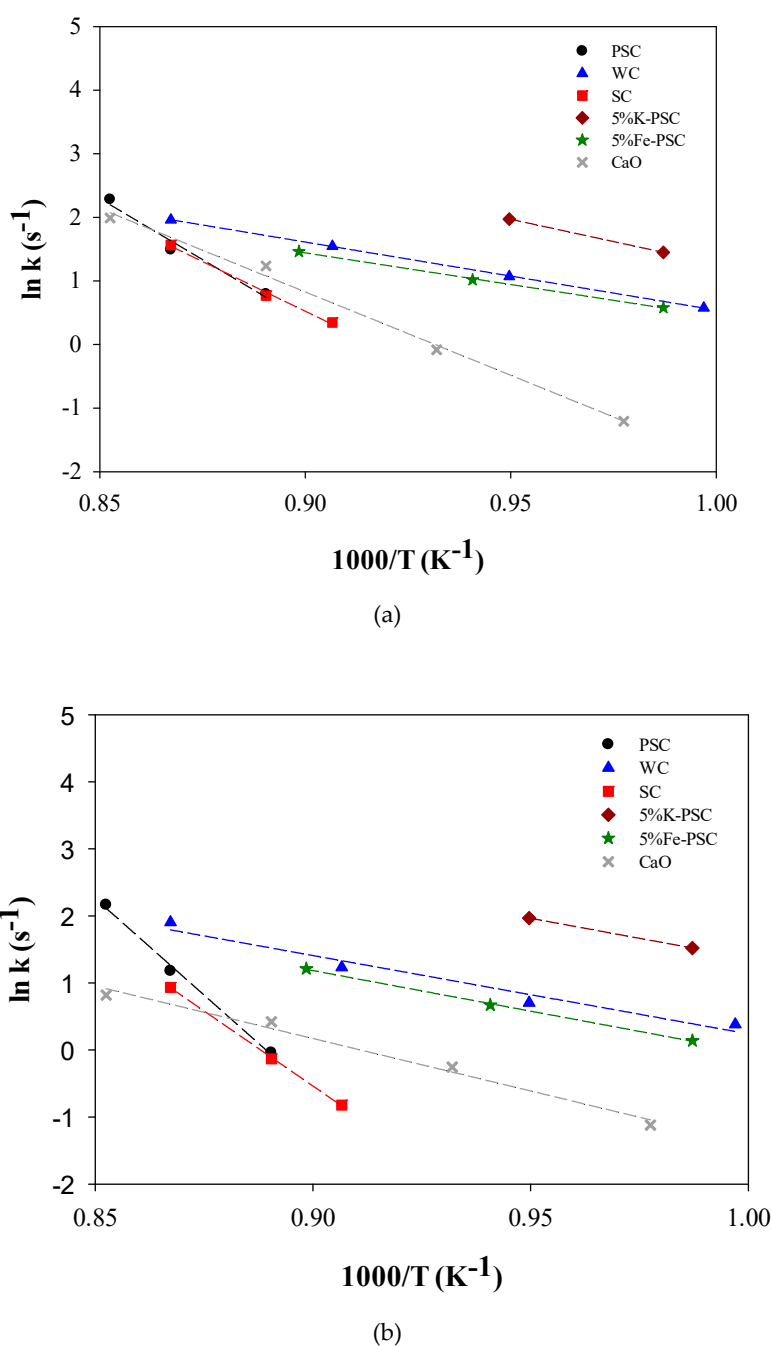


Figure 10. Temperature dependency of the apparent reaction rate constant according to Arrhenius' law. Calculation by; (a) toluene conversions; and (b) naphthalene conversions.

Table 4. Effect of temperature on fractional conversions and first-order rate constants for tar reforming over different catalysts. Calculation by toluene conversions and naphthalene conversions.

Tar Model Compound	Catalyst Type	T _r (°C)	X _T (-)	Ea (kJ/mol)	k ₀ (s ⁻¹)	R ² *
Toluene	PSC	850–900	0.31–0.81	318.9	1.44 × 10 ¹⁵	0.973
	WC	730–880	0.26–0.70	89.0	7.66 × 10 ⁴	0.999
	SC	830–880	0.21–0.56	259.7	2.73 × 10 ¹²	0.995
	5%K-PSC	740–780	0.51–0.70	116.3	4.22 × 10 ⁶	-
	5%Fe-PSC	740–850	0.26–0.52	82.7	3.26 × 10 ⁴	0.999
	CaO	750–950	0.14–0.98	218.0	4.06 × 10 ¹⁰	0.994
Naphthalene	PSC	850–900	0.15–0.77	478.9	1.76 × 10 ²²	0.996
	WC	730–880	0.22–0.68	97.2	1.51 × 10 ⁵	0.963
	SC	830–880	0.07–0.35	372.2	1.83 × 10 ¹⁷	0.999
	5%K-PSC	740–780	0.54–0.70	99.1	5.88 × 10 ⁵	-
	5%Fe-PSC	740–850	0.18–0.43	100.6	1.74 × 10 ⁵	0.999
	CaO	750–950	0.15–0.68	130.1	1.56 × 10 ⁶	0.986

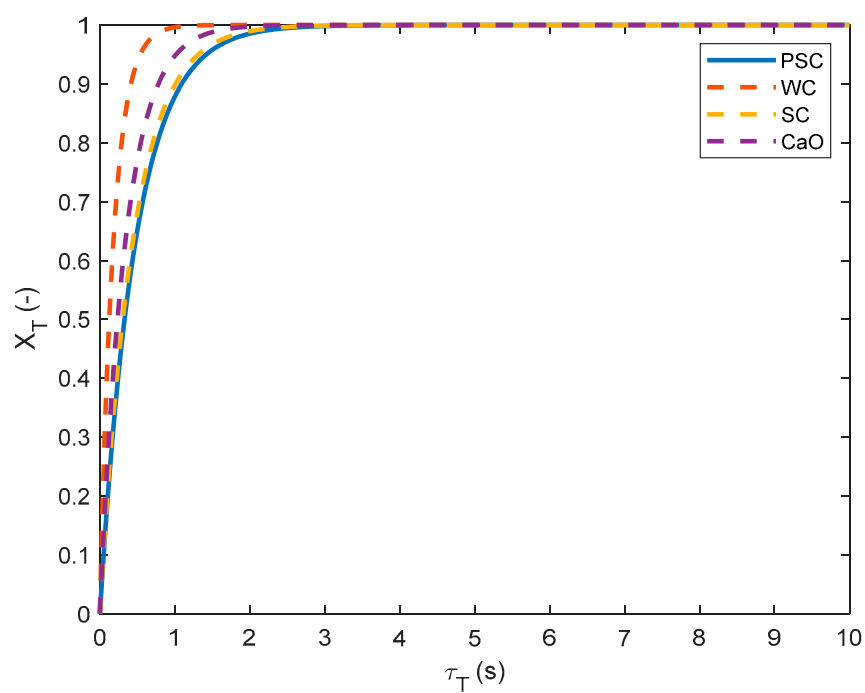
*R²: The percentage of the response variable variation that is explained by a linear model. This value is derived from Figure 10.

According to Figures 11 and 12, the theoretical residence time (τ_T , s) for the complete conversion of naphthalene is longer than that of toluene, indicating that this tertiary tar with a stable structure is harder to break down. At 850 °C, WC has the best catalytic activity for naphthalene reforming among natural materials, and CaO demonstrates a better activity than PSC and SC.

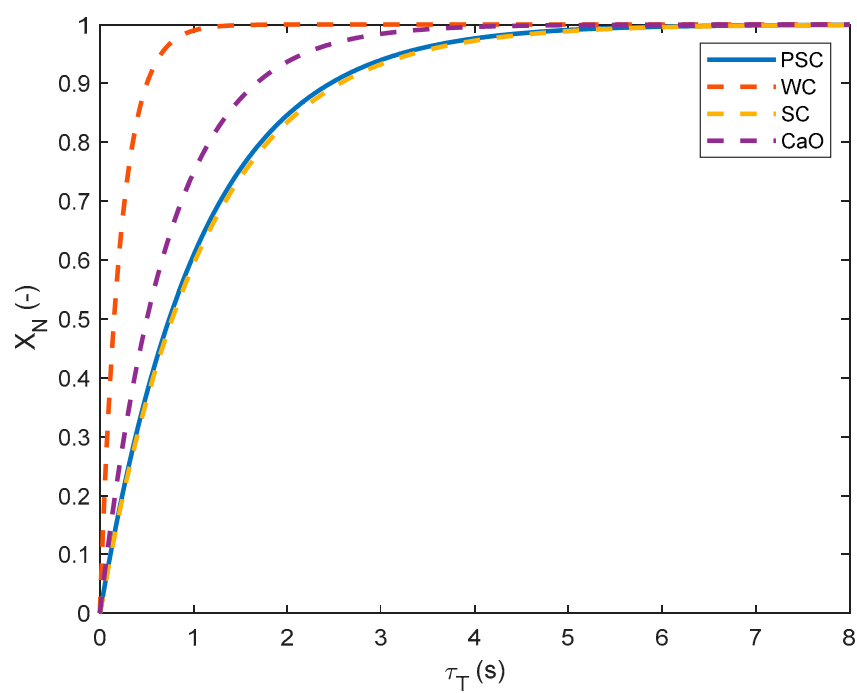
As temperature increases to 900 °C, four low-cost materials are much more inclined to reform toluene and naphthalene. X_T and X_N rapidly arrive at 100% conversion with less residence time than at 850 °C. It is also found that biochars possess better catalytic activity for naphthalene reforming than CaO at 900 °C, according to Figure 12. Among four materials, PSC exhibits an excellent activity for naphthalene reforming at 900 °C, which reached complete conversion at $\tau_T = 1.2$ s much shorter than 10.6 s at 850 °C. The temperature is then confirmed to be one of the most crucial parameters for tar reforming regarding the result. The bulk volume of PSC with the value above 3.33×10^{-4} m³ per m³ h⁻¹ of SEG-derived syngas is theoretically required for tar reforming at 900 °C, based on the kinetic constant of naphthalene reforming over PSC.

The advantage of loading with potassium and iron on biochar is that Ea for the reforming of tar model compounds becomes much lower (shown in Table 4), meaning that tar reforming over K- and Fe-PSC can be accomplished at more moderate temperatures compared to PSC. The energy consumption thus decreases for a long-time reforming. In order to avoid considerable mass loss of PSC due to gasification at high temperatures, metal-loaded PSC is, therefore, more suitable for low-temperature tar reforming. 5%K-PSC and 5%Fe-PSC are hence compared to PSC at a low temperature of 750 °C with the relationship between residence time and conversion, as can be seen in Figure 13. A complete conversion of naphthalene for 5%K- and Fe-loaded PSC is reached with $\tau_T = 1.7$ and 6.9 s, respectively, while PSC shows a weak activity with $X_N = 0.06$ at $\tau_T = 10$ s. In comparison to required τ_T (10.6 s) for complete conversion over PSC at 850 °C, 5%K-PSC and 5%Fe-PSC show still better catalytic activities at 750 °C, proving potassium and iron are prominent promoters for not only reducing the reforming temperature, but also significantly enhancing the catalytic activity of PSC.

On account of the above findings, PSC is applicable as tar-reforming catalysts at the high-temperature range around 900 °C, which can theoretically achieve complete tar conversion with short residence time. Besides, the catalytic activity of PSC can be enhanced after impregnated with potassium and iron. For design purposes, the mass of active materials required in the reformer for SEG derived syngas can be deduced from Figures 11–13 to approach the target conversion at specific temperatures.

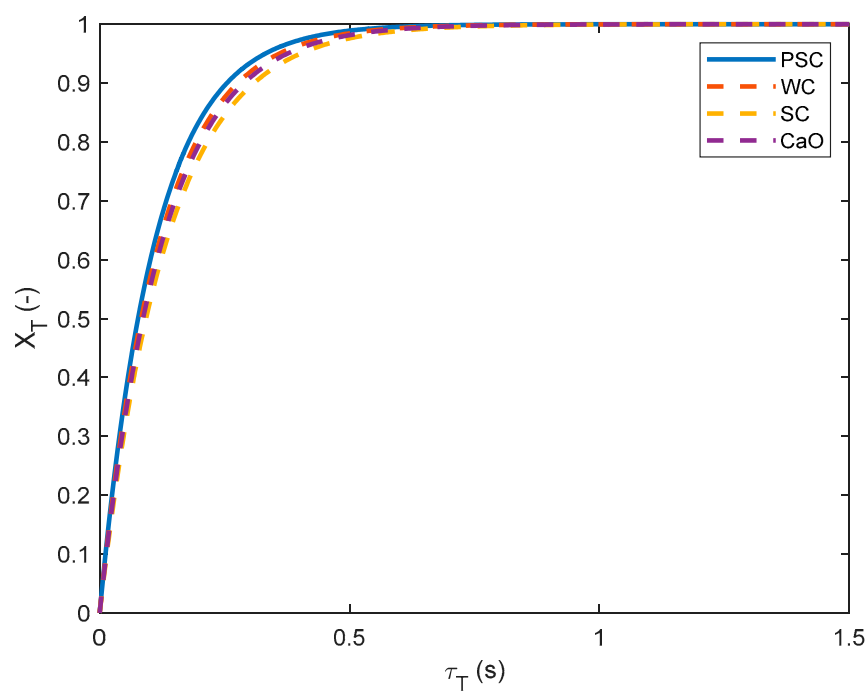


(a)

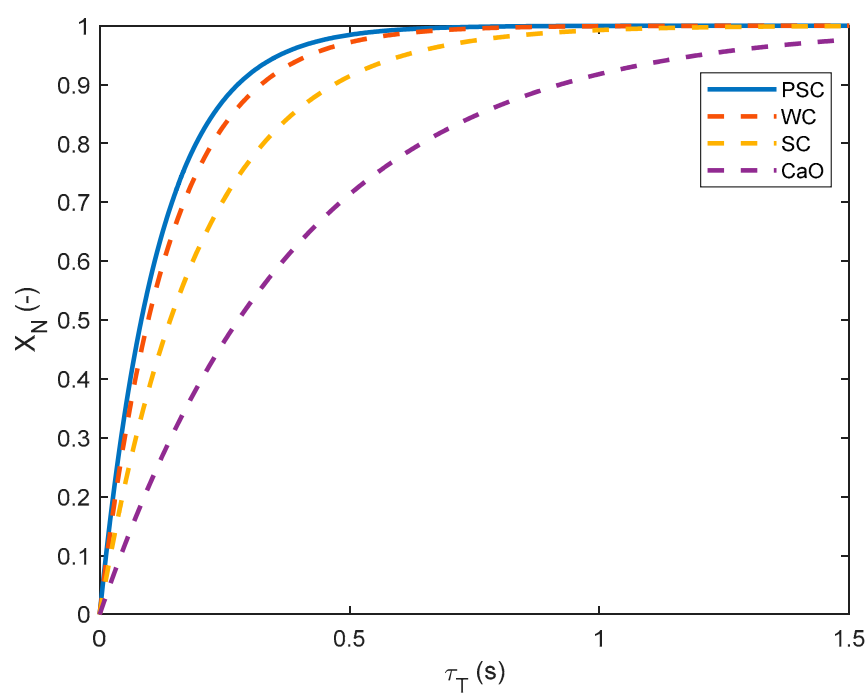


(b)

Figure 11. (a) Toluene; and (b) naphthalene conversion as a function of theoretical residence time at 850 °C for different active materials.

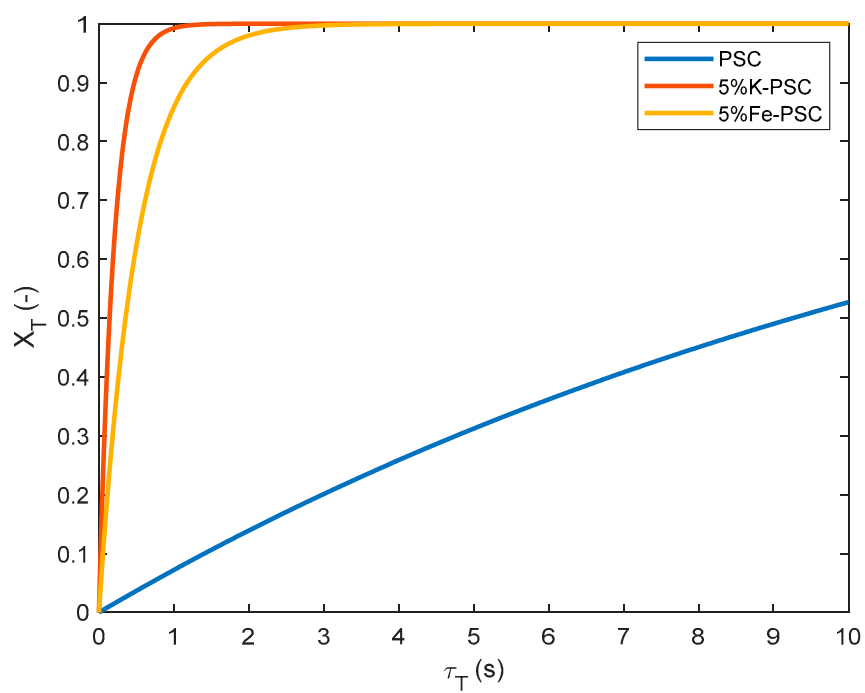


(a)

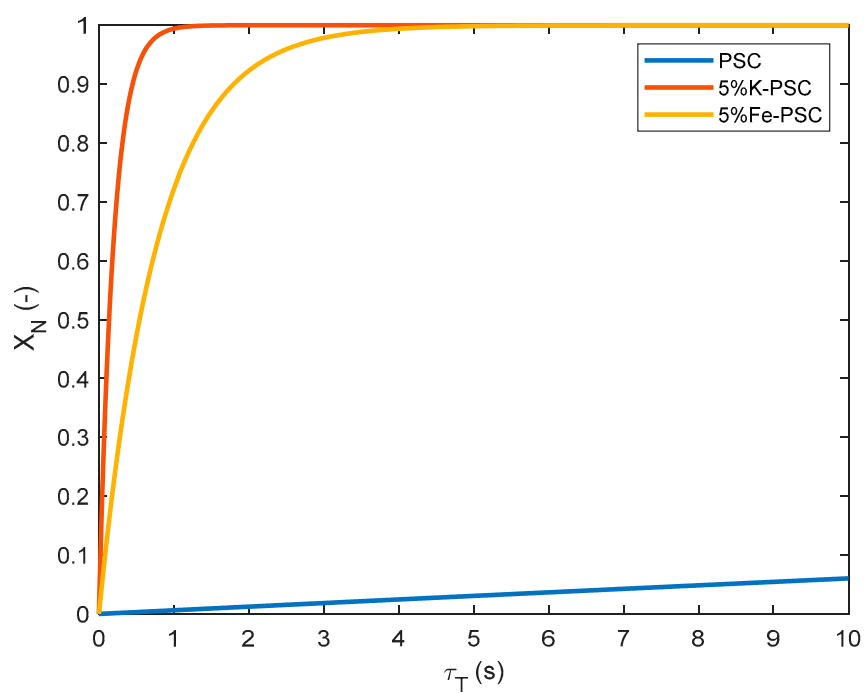


(b)

Figure 12. (a) Toluene; and (b) naphthalene conversion as a function of theoretical residence time at 900 °C for different active materials.



(a)



(b)

Figure 13. (a) Toluene; and (b) naphthalene conversion as a function of theoretical residence time at 750 °C for PSC, 5%K-PSC, and 5%Fe-PSC.

3. Material and Methods

3.1. Materials

PSs imported from Malaysia by Liang Xin Energy Co., Ltd. (New Taipei City, Taiwan) were carbonized at 450 °C in the self-generated atmosphere for 30 min with nitrogen to remove most of the volatiles. This range of temperature has also been applied as bio-oil production by pyrolysis of PSs. The temperature then rose to 850 °C, reaching the temperature range of tar reforming to produce final palm shell chars (PSCs). PSCs were then sieved to the size of 2–5 mm for tar reforming. Moreover, this research adopted a low-cost impregnation method with K_2CO_3 (99.5%, SHOWA CHEMICAL CO., LTD., Nihombashihoncho, Tokyo, Japan) and $Fe(NO_3)_3 \cdot 9H_2O$ (98%, VETEC, Merck KGaA, Darmstadt, HE, Germany) to prepare K- and Fe-loaded PSC. Solutions of potassium and iron salt, prepared by dissolving K_2CO_3 and $Fe(NO_3)_3 \cdot 9H_2O$ in an appropriate amount of DI water, were mixed with PSs for 12 h under continuous intense agitation using a magnetic stirrer, and then dried at 105 °C for 24 h. The amounts of K_2CO_3 and $Fe(NO_3)_3 \cdot 9H_2O$ added in the solution were decided by making K and Fe occupy 5 wt.% of the metal impregnated PS assuming that all potassium or iron ions in the solution could evenly cover on the surface of PSs. The metal impregnated PSs were subsequently pyrolyzed in a similar method as adopted for PSCs. K- and Fe-loaded PSC were named 5%K-PSC, and 5%Fe-PSC, respectively. Tar reforming was also carried out with wood char (WC), straw char (SC), and CaO as catalysts with similar pellet diameter (2–5 mm) to PSC to observe the difference of these materials by using them as tar-reforming catalysts. The same pyrolysis method was adopted for straw pellets (GIEE, National Taiwan University, Taipei, Taiwan) to manufacture SCs, while WCs were produced by pyrolysis of wood pellets (SCHARR WÄRME, Stuttgart, BW, Germany) in a fluidized bed at a constant temperature of 850 °C for 1 hr. The bed material of the SEG process, CaO, has been proved that it can reduce tar production and convert heavy tar into light tar. CaO, which is obtained from the calcination of limestone (Lhoist Germany Rheinkalk GmbH, Wülfrath, NW, Germany) at 900 °C, was also tested here as the reference catalyst representing mineral rock catalyst. The calcined limestone, which is regarded as “CaO” in this study, consisted of over 90% CaO.

3.2. Experiment Method

A high-temperature laboratory-scale catalytic tar reduction system capable of operating at various conditions was developed in this study, as shown in Figure 14. Low-cost materials (PSC, 5%K-PSC, 5%Fe-PSC, WC, SC, and CaO) were tested as the catalysts filled in the reactor. All pipes were heated up above 180 °C to avoid condensation of tar. A relevant test gas with 15 vol % H_2O , 7.5 vol % H_2 (99.9%, Westfalen AG, Münster, NW, Germany), and tar model compounds was premixed in N_2 (99.999%, Westfalen AG, Münster, NW, Germany) simulating the essential components of the raw syngas from the SEG process [2–4]. The tar model components were toluene (99.5%, Merck KGaA, Darmstadt, HE, Germany) and naphthalene (Riedel-de Haën AG, Seelze, NI, Germany), amounting to total tar concentration of circa $10 \text{ g m}^{-3}_{NTP}$. The residence times of the gas (τ_{NTP} , s) over the biochars and CaO were 0.17 and 0.51 s, respectively, calculated by the bulk volume of the catalyst bed (V_{bed} , m^3) divided by total flow rate (Q_{NTP} , $m^3 \text{ s}^{-1}$). Long-term tests of PSC, WC, and SC with 90 min reforming were conducted at different temperatures.

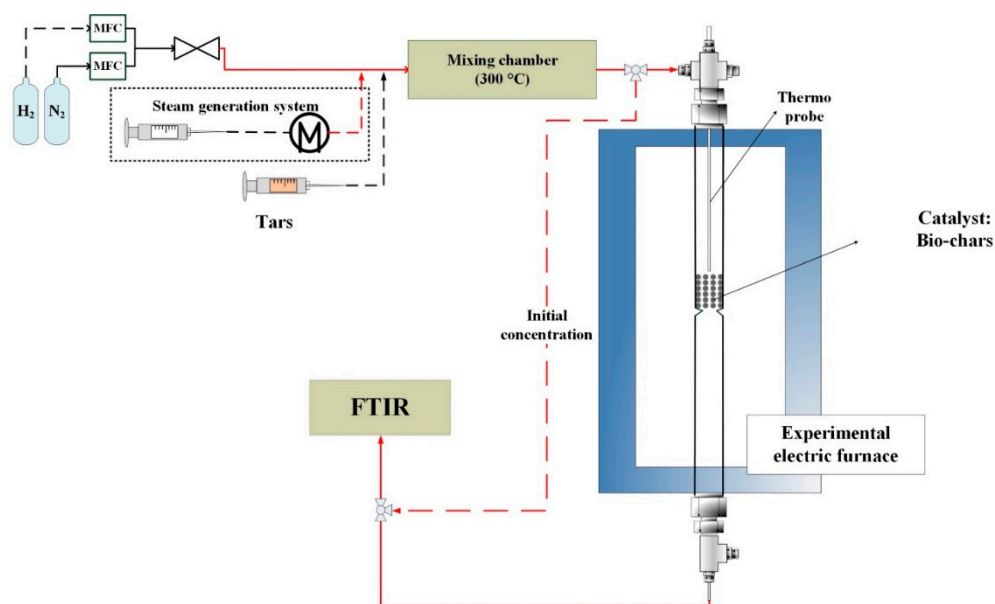


Figure 14. Diagram of tar reforming system.

3.3. Detection of Gas Components

By Fourier–transform infrared spectroscopy analyzer (FTIR–Gas analyzer, GASMET DX4000, Gasmet Technologies Oy, Mestarintie, Vantaa, Finland), continuous toluene and naphthalene concentrations were recorded, and concentrations of C_6H_6 , CO , CO_2 , and CH_4 were also detected with a transmitting pipe (5 m length) at 180 °C. The initial concentration was also recorded at the beginning of every test.

3.4. Analytical and Characterization Methods

Elemental, ultimate analyses and metal oxide compositions of biochars were performed following standard methods DIN (the German Institute for Standardization) EN ISO 18134–3, 18122, 18123, 16948, 16967, and 16994 [50]. Thermal gravimetric analysis (TGA) and derivative thermal gravimetric analysis (DTG) were tested in the same condition described by Chen et al. [32]. The porous structure of the char sample, including BET surface area, pore volume, and average pore diameter, was measured by an automatic volumetric analyzer (Micromeritics ASAP 2420, Micromeritics Instrument Corp., Norcross, GA, U.S.A.) using liquid N_2 as the adsorption agent. The catalyst sample was degassed at 200 °C to remove adsorbed contaminants and water vapor on the surface of the catalyst. The information of micropore and mesopore was calculated by the approaches of t-plot and Barrett-Joyner-Halenda (BJH) [51,52].

3.5. Toluene and Naphthalene Reforming

Many parallel and consecutive reactions can occur during toluene and naphthalene reforming in the environment with high steam concentration [53–55]. According to the global steam reforming reaction, toluene and naphthalene can react with steam to generate H_2 and CO :

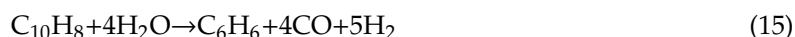


The Water-Gas-Shift reaction (WGS) takes place simultaneously:

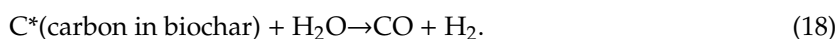


Some work in the literature suggested that Equations (11) and (12) may be divided into two different reactions in series: The solid carbonaceous deposition on the solid surface by tar polymerization or coke accumulation followed by the steam gasification/reforming of the carbonaceous solid [37]. It is worth mentioning that carbon deposition reactions highly depend on the temperature and the concentration of the oxidizing component (steam). When the reaction temperature is too low, or not enough steam is present, coke can quickly accumulate on the solid surface [56].

In the presence of steam and hydrogen, also other reactions should be considered during tar reforming. Toluene and naphthalene can react with steam to produce C_6H_6 , CO, and H_2 from the reaction of steam dealkylation (Equations (14) and (15)) or with hydrogen to form C_6H_6 and CH_4 owing to the hydrodealkylation reaction (Equations (16) and (17)) [57]:



Biochar can also go through steam reforming (gasification) during steam reforming of tar:



3.6. Calculation Formulas

The concentrations obtained from FTIR were able to quantify the present reagents and products. AS biochar was simultaneously gasified during the reforming of tar model compounds, carbon balance was hard to prove with the parallel production of carbon-containing species from biochar. As a result, CaO was also used as a reference catalyst for confirming that the experimental process in this study gave a credible carbon balance during the reforming. Figure 15 depicts the carbon balance of the reforming of tar model compounds over CaO at 850 °C between reacted tar model mixture and majorly produced carbon-containing species (CO , CO_2 , CH_4 , and C_6H_6). Since there is a good fit between carbon converted and carbon produced, a constant total volume flow rate before and after the reaction was then assumed in this study. Here, gasification of biochar catalysts was also assumed to have no influence on total volume flow.

Toluene conversion (X_T , -) and naphthalene conversion (X_N , -) were then computed using Equations (19), and (20), respectively,

$$X_T = \frac{y_{C7H8,in} - y_{C7H8,out}}{y_{C7H8,in}} \quad (19)$$

$$X_N = \frac{y_{C10H8,in} - y_{C10H8,out}}{y_{C10H8,in}} \quad (20)$$

where $y_{C7H8,in}$, ppmv = inlet toluene volume concentration, $y_{C7H8,out}$, ppmv = outlet toluene volume concentration, $y_{C10H8,in}$, ppmv = inlet naphthalene volume concentration, and $y_{C10H8,out}$, ppmv = outlet naphthalene volume concentration.

Benzene selectivity (S_{C6H6} , -) was defined by Equation (21), assuming that benzene all produced from tar model compounds,

$$S_{C6H6} = \frac{6 \cdot y_{C6H6}}{7 \cdot (y_{C7H8,in} - y_{C7H8,out}) + 10 \cdot (y_{C10H8,in} - y_{C10H8,out})} \quad (21)$$

where y_i (ppmv) represents the outlet volume concentration of the product i (y_{C6H6} : the outlet volume concentration of benzene.)

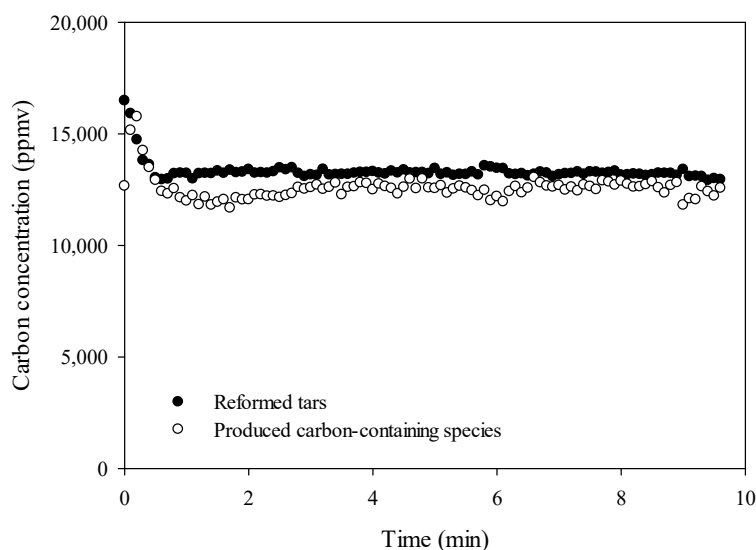


Figure 15. Carbon balance of toluene and naphthalene reforming over CaO at 850 °C. (Reformed toluene and naphthalene: $7 \cdot (y_{C7H8,in} - y_{C7H8,out}) + 10 \cdot (y_{C10H8,in} - y_{C10H8,out})$; Produced carbon-containing species: $y_{CO} + y_{CO_2} + y_{CH_4} + 6 \cdot y_{C_6H_6}$).

4. Conclusions

Pyrolysis of PS removes most volatiles of PS and produces PSC with a high surface area and good hydrophobicity. PSC performed significantly in tar reforming at 900 °C, with a theoretically required bulk volume of $3.33 \times 10^{-4} \text{ m}^3$, for the complete tar conversion per $\text{m}^3 \text{ h}^{-1}$ of SEG-derived syngas, which proves that it has a good potential applied in a tar reformer after SEG process. As for the reforming selectivity, toluene and naphthalene over PSC are mainly decomposed to light components with low benzene selectivity. Parallel gasification of biochars during the reforming of tar model compounds is highly related to the activation and deactivation of biochars. Initial gasification can increase the surface area and micropores. However, mass loss and pore collapsing after continuous gasification lead to the deactivation of biochars. With low reactivity to steam, palm shell char is a suitable choice for applying the catalyst, compared to wood char and straw char, as it avoids drastic mass loss in the long-term toluene and naphthalene reforming. Moreover, it is worth developing K- and Fe- loaded palm shell char for reducing the reforming temperature. These metal promoters significantly enhance the catalytic activity of palm shell char, while intense gasification carried out on potassium loaded palm shell char results in a rapid mass loss. Iron is a relatively tender promoter on the palm shell char suitable for long-term operation with a quick activation only at the very beginning during the reforming of toluene and naphthalene mixture.

Author Contributions: Y.-H.C. and M.S. conceived and designed the experiments; Y.-H.C. performed the experiments; Y.-H.C. analyzed the data; C.-C.C. and G.S. contributed reagents/materials/analysis tools; M.S. and C.-Y.C. discussed the results and provided the suggestion. Y.-H.C. wrote the paper. All authors have read and agreed to the published version of the manuscript.

Funding: This research was funded by the project NuCA (0324342A) of the German Ministry of Economic Affairs and Energy (BMWi).

Acknowledgments: The authors gratefully acknowledge the support from DAAD (German Academic Exchange Service) and the project NuCA (0324342A) funded by the German Ministry of Economic Affairs and Energy (BMWi).

Conflicts of Interest: The authors declare no conflict of interest.

References

1. Hawthorne, C.; Poboss, N.; Dieter, H.; Gredinger, A.; Zieba, M.; Scheffknecht, G. Operation and results of a 200-kWth dual fluidized bed pilot plant gasifier with adsorption-enhanced reforming. *Biomass Conv. Bioref.* **2012**, *2*, 217–227. [\[CrossRef\]](#)
2. Schweitzer, D.; Beirrow, M.; Gredinger, A.; Armbrust, N.; Waizmann, G.; Dieter, H.; Scheffknecht, G. Pilot-Scale Demonstration of Oxy-SER steam Gasification: Production of Syngas with Pre-Combustion CO₂ Capture. *Energy Procedia* **2016**, *86*, 56–68. [\[CrossRef\]](#)
3. Poboss, N. Experimental investigation of the absorption enhanced reforming of biomass in a 20 kWth dual fluidized bed system. *Int. J. Thermodyn.* **2012**, *15*. [\[CrossRef\]](#)
4. Milne, T.A.; Evans, R.J.; Abatzoglou, N. *Biomass Gasifier “Tars”: Their Nature, Formation, and Conversion*; National Renewable Energy Laboratory: Golden, CO, USA, 1998.
5. Bridgwater, A.V. The technical and economic feasibility of biomass gasification for power generation. *Fuel* **1995**, *74*, 631–653. [\[CrossRef\]](#)
6. Jess, A. Catalytic upgrading of tarry fuel gases: A kinetic study with model components. *Chem. Eng. Process* **1996**, *35*, 487–494. [\[CrossRef\]](#)
7. Depner, H. Untersuchungen Zur Katalytischen Umsetzung Flüchtiger Schwelprodukte in Rohgasen Der Verkokung Und Vergasung Fester Brennstoffe. Ph.D. Thesis, TH Karlsruhe, Karlsruhe, Germany, 1998.
8. Speidel, M.; Fischer, H. Steam reforming of tars at low temperature and elevated pressure for model tar component naphthalene. *Int. J. Hydrog. Energy* **2016**, *41*, 12920–12928. [\[CrossRef\]](#)
9. Armbrust, N.; Poboss, N.; Eder, T.; Zieba, M.; Scheffknecht, G. Comparison of Two Methods of Sampling and Analyzing Tars during AER Biomass Gasification. In Proceedings of the 19th European Biomass Conference and Exhibition, Berlin, Germany, 6–10 June 2011.
10. Diehl, A. Experimentelle Untersuchung der Reformierung von Teeren an Katalytisch Aktiven Substanzen. Ph.D. Thesis, Uni Stuttgart, Stuttgart, Germany, 2012.
11. Soukup, G.; Pfeifer, C.; Kreuzeder, A.; Hofbauer, H. In Situ CO₂ Capture in a Dual Fluidized Bed Biomass Steam Gasifier—Bed Material and Fuel Variation. *Chem. Eng. Technol.* **2009**, *32*, 348–354. [\[CrossRef\]](#)
12. Pfeifer, C.; Koppatz, S.; Hofbauer, H. Steam gasification of various feedstocks at a dual fluidised bed gasifier: Impacts of operation conditions and bed materials. *Biomass Conv. Bioref.* **2011**, *1*, 39–53. [\[CrossRef\]](#)
13. Steiert, S. *FuE-Plattform “Biomass-to-Gas”—Energetische Nutzung biogener Reststoffe mit AER-Technologie zur Poly-Generation von Strom, Wasserstoff, Erdgassubstitut und Wärme, Schlussbericht*; Zentrums für Sonnenenergie-und Wasserstoff-Forschung Baden-Württemberg (ZSW): Stuttgart, Germany, 2013.
14. Aznar, M.P.; Caballero, M.A.; Gil, J.; Martín, J.A.; Corella, J. Commercial Steam Reforming Catalysts To Improve Biomass Gasification with Steam–Oxygen Mixtures. 2. Catalytic Tar Removal. *Ind. Eng. Chem. Res.* **1998**, *37*, 2668–2680. [\[CrossRef\]](#)
15. Abu El-Rub, Z.; Bramer, E.A.; Brem, G. Review of Catalysts for Tar Elimination in Biomass Gasification Processes. *Ind. Eng. Chem. Res.* **2004**, *43*, 6911–6919. [\[CrossRef\]](#)
16. Kostyniuk, A.; Grilc, M.; Likozar, B. Catalytic Cracking of Biomass-Derived Hydrocarbon Tars or Model Compounds To Form Biobased Benzene, Toluene, and Xylene Isomer Mixtures. *Ind. Eng. Chem. Res.* **2019**, *58*, 7690–7705. [\[CrossRef\]](#)
17. Zeng, X.; Ueki, Y.; Yoshiie, R.; Naruse, I.; Wang, F.; Han, Z.; Xu, G. Recent progress in tar removal by char and the applications: A comprehensive analysis. *Carbon Resour. Convers.* **2020**, *3*, 1–18. [\[CrossRef\]](#)
18. Prasertsan, S.; Prasertsan, P. Biomass residues from palm oil mills in Thailand: An overview on quantity and potential usage. *Biomass Bioenergy* **1996**, *11*, 387–395. [\[CrossRef\]](#)
19. Ani, F.N.; Zailani, R. Characteristics of Pyrolysis Oil and Char from Oil Palm Shells. In *Developments in Thermochemical Biomass Conversion*, 1st ed.; Bridgwater, A.V., Boocock, D.G.B., Eds.; Springer Netherlands: Dordrecht, The Netherlands, 1997; pp. 425–432.
20. Kim, S.-J.; Jung, S.-H.; Kim, J.-S. Fast pyrolysis of palm kernel shells: Influence of operation parameters on the bio-oil yield and the yield of phenol and phenolic compounds. *Bioresour. Technol.* **2010**, *101*, 9294–9300. [\[CrossRef\]](#) [\[PubMed\]](#)
21. Wan Daud, W.M.A.; Ali, W.S.W.; Sulaiman, M.Z. Effect of activation temperature on pore development in activated carbon produced from palm shell. *J. Chem. Technol. Biotechnol.* **2003**, *78*, 1–5. [\[CrossRef\]](#)

22. Mani, S.; Kastner, J.R.; Juneja, A. Catalytic decomposition of toluene using a biomass derived catalyst. *Fuel Process. Technol.* **2013**, *114*, 118–125. [\[CrossRef\]](#)
23. Feng, D.; Zhao, Y.; Zhang, Y.; Zhang, Z.; Zhang, L.; Sun, S. In-situ steam reforming of biomass tar over sawdust biochar in mild catalytic temperature. *Biomass Bioenergy* **2017**, *107*, 261–270. [\[CrossRef\]](#)
24. Feng, D.; Zhao, Y.; Zhang, Y.; Sun, S.; Meng, S.; Guo, Y.; Huang, Y. Effects of K and Ca on reforming of model tar compounds with pyrolysis biochars under H₂O or CO₂. *Chem. Eng. J.* **2016**, *306*, 422–432. [\[CrossRef\]](#)
25. Feng, D.; Zhao, Y.; Zhang, Y.; Zhang, Z.; Che, H.; Sun, S. Experimental comparison of biochar species on in-situ biomass tar H₂O reforming over biochar. *Int. J. Hydrog. Energy* **2017**, *42*, 24035–24046. [\[CrossRef\]](#)
26. Feng, D.; Zhao, Y.; Zhang, Y.; Zhang, Z.; Sun, S. Roles and fates of K and Ca species on biochar structure during in-situ tar H₂O reforming over nascent biochar. *Int. J. Hydrog. Energy* **2017**, *42*, 21686–21696. [\[CrossRef\]](#)
27. Klinghoffer, N.B.; Castaldi, M.J.; Nzihou, A. Catalyst Properties and Catalytic Performance of Char from Biomass Gasification. *Ind. Eng. Chem. Res.* **2012**, *51*, 13113–13122. [\[CrossRef\]](#)
28. Kastner, J.R.; Mani, S.; Juneja, A. Catalytic decomposition of tar using iron supported biochar. *Fuel Process. Technol.* **2015**, *130*, 31–37. [\[CrossRef\]](#)
29. Nordgreen, T.; Liliedahl, T.; Sjoström, K. Metallic iron as a tar breakdown catalyst related to atmospheric, fluidised bed gasification of biomass. *Fuel* **2006**, *85*, 689–694. [\[CrossRef\]](#)
30. Chen, Y.-H.; Schmid, M.; Waizmann, G.; Hafner, S.; Scheffknecht, G. Tar Reforming over CAO and Straw Char Produced Inherently in Steam-oxygen Biomass Gasification Processes Using Toluene as Model Component. In Proceedings of the 27th European Biomass Conference and Exhibition, Lisbon, Portugal, 27–30 May 2019. [\[CrossRef\]](#)
31. Klinghoffer, N.B.; Castaldi, M.J.; Nzihou, A. Influence of char composition and inorganics on catalytic activity of char from biomass gasification. *Fuel* **2015**, *157*, 37–47. [\[CrossRef\]](#)
32. Chen, Y.-H.; Chang, C.-C.; Chang, C.-Y.; Yuan, M.-H.; Ji, D.-R.; Shie, J.-L.; Lee, C.-H.; Chen, Y.-H.; Chang, W.-R.; Yang, T.-Y.; et al. Production of a solid bio-fuel from waste bamboo chopsticks by torrefaction for cofiring with coal. *J. Anal. Appl. Pyrolysis* **2017**, *126*, 315–322. [\[CrossRef\]](#)
33. Kajita, M.; Kimura, T.; Norinaga, K.; Li, C.-Z.; Hayashi, J.-i. Catalytic and Noncatalytic Mechanisms in Steam Gasification of Char from the Pyrolysis of Biomass. *Energy Fuels* **2010**, *24*, 108–116. [\[CrossRef\]](#)
34. Guo, F.; Liu, Y.; Wang, Y.; Li, X.; Li, T.; Guo, C. Pyrolysis kinetics and behavior of potassium-impregnated pine wood in TGA and a fixed-bed reactor. *Energy Convers. Manag.* **2016**, *130*, 184–191. [\[CrossRef\]](#)
35. Industrial Development Bureau of Taiwan. *Regional Energy Resource Integration and Efficiency Enhancement Demonstration Counseling Project*; Industrial Development Bureau: Taipei, Taiwan, 2016.
36. Prakash Kumar, B.G.; Shivakamy, K.; Miranda, L.R.; Velan, M. Preparation of steam activated carbon from rubberwood sawdust (*Hevea brasiliensis*) and its adsorption kinetics. *J. Hazard. Mater.* **2006**, *136*, 922–929. [\[CrossRef\]](#)
37. Fuentes-Cano, D.; Gómez-Barea, A.; Nilsson, S.; Ollero, P. Decomposition kinetics of model tar compounds over chars with different internal structure to model hot tar removal in biomass gasification. *Chem. Eng. J.* **2013**, *228*, 1223–1233. [\[CrossRef\]](#)
38. Nilsson, S.; Gomez-Barea, A.; Fuentes Cano, D. Gasification reactivity of char from dried sewage sludge in a fluidized bed. *Fuel* **2012**, *92*, 346–353. [\[CrossRef\]](#)
39. Zeng, X.; Wang, F.; Han, Z.; Han, J.; Zhang, J.; Wu, R.; Xu, G. Assessment of char property on tar catalytic reforming in a fluidized bed reactor for adopting a two-stage gasification process. *Appl. Energy* **2019**, *248*, 115–125. [\[CrossRef\]](#)
40. Suzuki, T.; Nakajima, H.; Ikenaga, N.-o.; Oda, H.; Miyake, T. Effect of mineral matters in biomass on the gasification rate of their chars. *Biomass Conv. Bioref.* **2011**, *1*, 17–28. [\[CrossRef\]](#)
41. Yip, K.; Tian, F.; Hayashi, J.-I.; Wu, H. Effect of Alkali and Alkaline Earth Metallic Species on Biochar Reactivity and Syngas Compositions during Steam Gasification. *Energy Fuels* **2010**, *24*, 173–181. [\[CrossRef\]](#)
42. Yu, J.; Tian, F.; Chow, M.; McKenzie, L.; Li, C. Effect of iron on the gasification of Victorian brown coal with steam: enhancement of hydrogen production. *Fuel* **2006**, *85*, 127–133. [\[CrossRef\]](#)
43. Guo, F.; Liu, Y.; Liu, Y.; Guo, C. Catalytic reforming of tar using corncob char and char-supported potassium catalysts. *J. Therm. Anal. Calorim.* **2017**, *130*, 1297–1306. [\[CrossRef\]](#)
44. Fu, P.; Hu, S.; Xiang, J.; Yi, W.; Bai, X.; Sun, L.; Su, S. Evolution of char structure during steam gasification of the chars produced from rapid pyrolysis of rice husk. *Bioresour. Technol.* **2012**, *114*, 691–697. [\[CrossRef\]](#)

45. Song, Y.; Wang, Y.; Hu, X.; Hu, S.; Xiang, J.; Zhang, L.; Zhang, S.; Min, Z.; Li, C.-Z. Effects of volatile-char interactions on in situ destruction of nascent tar during the pyrolysis and gasification of biomass. Part I. Roles of nascent char. *Fuel* **2014**, *122*, 60–66. [CrossRef]
46. Song, Y.; Wang, Y.; Hu, X.; Xiang, J.; Hu, S.; Mourant, D.; Li, T.; Wu, L.; Li, C.-Z. Effects of volatile-char interactions on in-situ destruction of nascent tar during the pyrolysis and gasification of biomass. Part II. Roles of steam. *Fuel* **2015**, *143*, 555–562. [CrossRef]
47. Ducouso, M.; Weiss-Hortala, E.; Nzihou, A.; Castaldi, M.J. Reactivity enhancement of gasification biochars for catalytic applications. *Fuel* **2015**, *159*, 491–499. [CrossRef]
48. Zhang, Y.; Feng, D.; Zhao, Y.; Dong, H.; Chang, G.; Quan, C.; Sun, S.; Qin, Y. Evolution of Char Structure During In-Situ Biomass Tar Reforming: Importance of the Coupling Effect Among the Physical-Chemical Structure of Char-Based Catalysts. *Catalysts* **2019**, *9*, 711. [CrossRef]
49. El-Rub, Z.A.; Bramer, E.A.; Brem, G. Experimental comparison of biomass chars with other catalysts for tar reduction. *Fuel* **2008**, *87*, 2243–2252. [CrossRef]
50. The German Institute for Standardization: DIN EN ISO 18134-3, 18122, 18123, 16948, 16967, and 16994. Available online: <https://www.din.de/de> (accessed on 4 November 2019).
51. Barrett, E.P.; Joyner, L.G.; Halenda, P.P. The Determination of Pore Volume and Area Distributions in Porous Substances. I. Computations from Nitrogen Isotherms. *J. Am. Chem. Soc.* **1951**, *73*, 373–380. [CrossRef]
52. Storck, S.; Bretinger, H.; Maier, W.F. Characterization of micro- and mesoporous solids by physisorption methods and pore-size analysis. *Appl. Catal. A* **1998**, *174*, 137–146. [CrossRef]
53. Taralas, G.; Kontominas, M.G. Kinetic modelling of VOC catalytic steam pyrolysis for tar abatement phenomena in gasification/pyrolysis technologies. *Fuel* **2004**, *83*, 1235–1245. [CrossRef]
54. Swierczynski, D.; Libs, S.; Courson, C.; Kiennemann, A. Steam reforming of tar from a biomass gasification process over Ni/olivine catalyst using toluene as a model compound. *Appl. Catal. B* **2007**, *74*, 211–222. [CrossRef]
55. Taralas, G.; Kontominas, M.G. Numerical modeling of tar species/VOC dissociation for clean and intelligent energy production. *Energy Fuels* **2005**, *19*, 87–93. [CrossRef]
56. Shekhawat, D.; Spivey, J.J.; Berry, D.A. *Fuel Cells: Technologies for Fuel Processing*, 1st ed.; Elsevier Science: Amsterdam, The Netherlands, 2011.
57. Taralas, G.; Kontominas, M.G.; Kakatsios, X. Modeling the thermal destruction of toluene (C₇H₈) as tar-related species for fuel gas cleanup. *Energy Fuels* **2003**, *17*, 329–337. [CrossRef]



© 2020 by the authors. Licensee MDPI, Basel, Switzerland. This article is an open access article distributed under the terms and conditions of the Creative Commons Attribution (CC BY) license (<http://creativecommons.org/licenses/by/4.0/>).